Supramolecular Chemistry

Rare and Diverse Binding Modes Introduced through Mechanical Bonding**

David A. Leigh, Paul J. Lusby, Alexandra M. Z. Slawin, and D. Barney Walker*

Interest in catenanes and rotaxanes has largely focused on the stimuli-induced change in the position of their components for possible exploitation in molecular devices,[1] but other properties and features of these architectures are becoming apparent.[2] Here, we report a previously unrecognized consequence of kinetic stabilization of an otherwise unfavorable association of molecular fragments through mechanical bonding (Figure 1). The raised energy of the interlocked components—brought about by the enforced high local concentration of convergent functional groups, the limitation in the number of conformations and co-conformations that each component can adopt, and the poor solvation of their inner surfaces—facilitates (kinetically and thermodynamically) the formation of internal and external binding motifs that are either not observed or much weaker when the same groups are not confined in this way. The effect is illustrated through a remarkable series of binding modes (including orthogonal bifurcated pyridine–pyridine hydrogen bonding,

[*] Prof. D. A. Leigh, Dr. P. J. Lusby, D. B. Walker
School of Chemistry
University of Edinburgh
The King's Buildings
West Mains Road, Edinburgh EH9 3JJ (UK)
Fax: (+44) 131-667-9085
E-mail: david.leigh@ed.ac.uk
Prof. A. M. Z. Slawin
School of Chemistry
University of St. Andrews
Purdie Building, St. Andrews, Fife KY16 9ST (UK)

[**] We thank Anne-Marie Fuller for the synthesis of H_2**4**. This work was supported by the European Union Future and Emerging Technology Program MechMol and by the EPSRC.

Supporting information for this article is available on the WWW under http://www.angewandte.org or from the author.

 DOI: 10.1002/anie.200500004

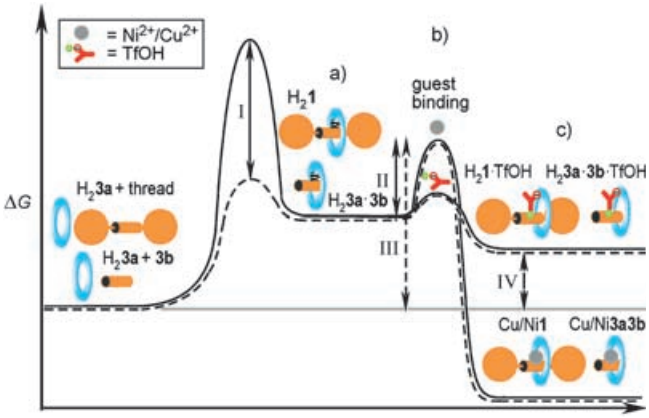

Figure 1. Effects of kinetic stabilization of an otherwise unfavorable association of molecular fragments through mechanical bonding. a) The kinetic stabilization (I) of a mechanically interlocked architecture that features only weakly attractive interactions between the macrocycle and thread permits noncovalent interactions to be observed (as in H_2**1**) which are too weak to stabilize the corresponding host–guest complex (H_2**3a**·**3b**). b) For a rotaxane that is not thermodynamically stable with respect to its free components, the activation energy for tertiary component complex formation is lower than for the analogous noninterlocked system (barrier II is less than III). This arises because the entropic cost of bringing the two components of the rotaxane together has already been paid, some degrees of freedom of the components are already restricted in the mechanically interlocked architecture, and the desolvation of the internal rotaxane surfaces is less energetically demanding than those of the free components. c) The higher energy of such a rotaxane means that a host–guest complex which involves the rotaxane can be favorable (e.g. H_2**1**·TfOH) even when the equivalent trimolecular complex (H_2**3a**·**3b**·TfOH) is not (IV). It also ensures that metal complexes derived from such rotaxanes, such as Cu**1** and Ni**1**, are inherently thermodynamically more stable than the analogous complexes derived from noninterlocked fragments and, in principle, kinetically easier to form. The association/dissociation pathways are shown by black solid (interlocked components) and dashed (noninterlocked components) lines; the horizontal gray line corresponds to the free energy of the nonassociated individual components.

cooperative binding to a sulfonic acid guest through deprotonation by one component and anion–amide hydrogen bonding by the other, enforced square-pyramidal coordination of Cu^{II} and Ni^{II}, and second-sphere coordination in a square-planar $Pd^{II}Cl$ complex) exhibited in solution and the solid state by a [2]rotaxane and an analogous [2]catenane, but not seen with either threadable (but nonmechanically interlocked) versions of the components or flexible covalently bonded systems (Figure 2).

Most catenanes and rotaxanes are synthesized by utilizing templates to thermodynamically favor interlocking,[1a] but subsequent removal of the template can leave a molecule that is energetically unstable with respect to the noninterlocked components and is only held intact by virtue of the mechanical bond. We recently described[3] the assembly of a mechanically interlocked architecture about a Pd^{II} template to give a square-planar [2]rotaxane–metal coordination complex, Pd**1**.[4] We were intrigued to find that upon protic demetalation of the complex to give H_2**1**, the ^{1}H NMR spectrum in $CDCl_3$ indicated significant intercomponent hydrogen bonding between the amide groups of the macrocycle and the pyridine nitrogen atom of the rotaxane thread (the protons of the amide groups in the macrocycle appear 1.7 ppm downfield relative to the corresponding protons in the free macrocycle). Such a binding motif, which requires essentially orthogonal pyridine rings with the nitrogen atoms bridged by bifurcated hydrogen bonds, is extremely rare (a search of the Cambridge Crystallographic Database reveals only one other example[5]) but is somewhat reminiscent of the hydrogen bonding that occurs at 90° to the plane of the lone pairs of amide groups in threads seen extensively in other hydrogen-bonded rotaxanes.[6] Slow cooling of a hot, saturated solution of H_2**1** in acetonitrile/chloroform (10:1) yielded single crystals that were of sufficient quality to confirm the interaction in the solid state by X-ray crystallography (Figure 3a, b) but were inadequate to confidently characterize the interaction in detail.[7] However, when we prepared a [2]catenane that incorporated the same functional groups, H_2**2**, a similar noncovalent interaction was observed in solution in $CDCl_3$ and, in this case, single crystals of excellent quality were obtained by slow cooling of a hot, saturated solution of H_2**2** in acetonitrile. The solid-state structure of H_2**2** (Figure 3c) closely mirrors the hydrogen-bonding motif seen in the crystal structure of H_2**1**, with unsymmetrical intercomponent hydrogen-bond distances (2.28 and 3.10 Å in H_2**2**; 2.3 and 2.8 Å in H_2**1**) and the angle between the planes of the

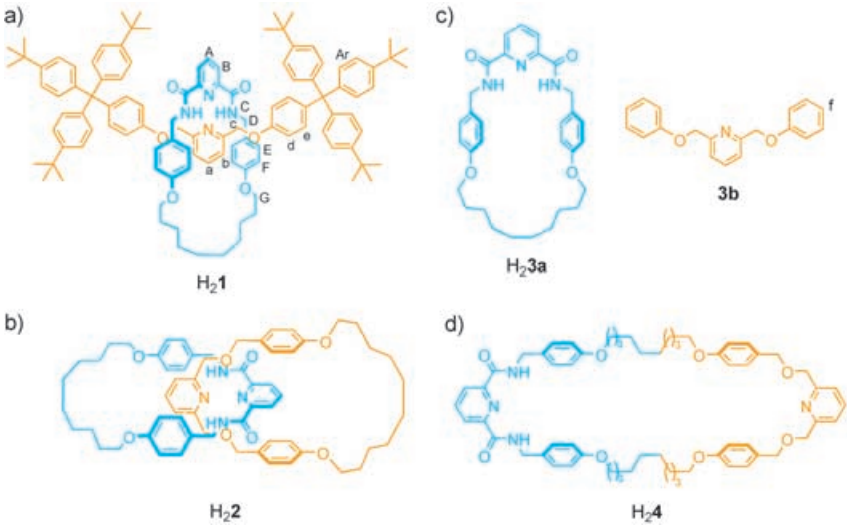

Figure 2. Different ways of linking a 2,6-dialkylpyridine unit with a 2,6-dicarboxamidepyridine unit which lead to significantly different noncovalent binding properties: a) on different components within a [2]rotaxane architecture, H_2**1**; b) on different components within a [2]catenane architecture, H_2**2**; c) on separate threadable, but not mechanically interlocked, molecular components H_2**3a** and **3b**; and d) on a flexible but wholly covalently bonded system, H_2**4**. For ^{1}H NMR spectroscopic assignments (see Figure 4), hydrogen atoms have been labeled A–G and a–f/Ar for the macrocycle and thread, respectively.

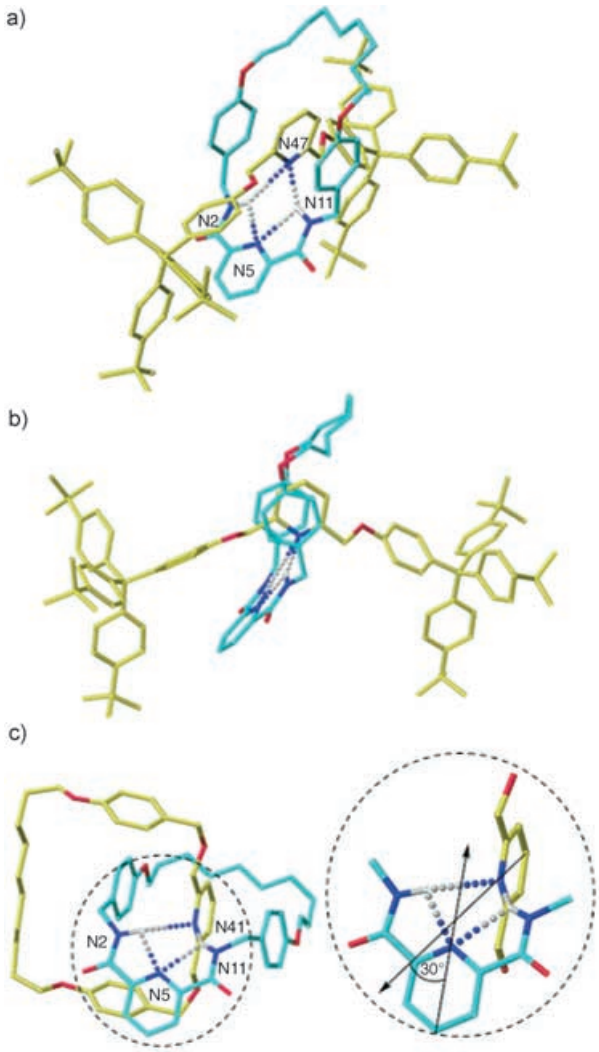

Figure 3. X-ray crystal structures[7] of [2]rotaxane H_2**1** and [2]catenane H_2**2**: a) H_2**1** (twisted view); b) H_2**1** (side view which shows the macrocycle circumscribing the pyridine residue of the thread; disorder in the alkyl chain region and solvent molecules, not the central hydrogen-bonding region, results in a high overall *R* factor of 33%); c) H_2**2** (*R* factor <5%; the intercomponent hydrogen-bond motif mirrors that shown in (a) and (b)). Inset: the lone pairs of the pyridine nitrogen atoms do not point directly at each other, but are tilted 30.0° apart. C (macrocycle) turquoise; C (thread) yellow; O red; N dark blue; H white. For clarity only nitrogen-bound hydrogen atoms are shown. Selected bond lengths [Å] for H_2**1**: N2H–N5 2.4; N11H–N5 2.6; N2H–N47 2.8; N11H–N47 2.3. Selected bond angles [°] for H_2**1**: N2H-N5 151; N11H-N5 153; N2H-N47 96; N11H-N47 108. Selected bond lengths [Å] for H_2**2**: N2H–N5 2.18; N11H–N5 2.33; N2H–N41 2.28; N11H–N41 3.10. Selected bond angles [°] for H_2**2**: N2H-N5 107.1; N11H-N5 102.2; N2H-N41 146.5; N11H-N41 129.0.

pyridine rings nearly orthogonal (90.7° in H_2**2**; 82° in H_2**1**) but tilted (30.0° in H_2**2** (Figure 3c, inset); 34° in H_2**1**) away from linearity to avoid too close an interaction between the lone pairs on the pyridine nitrogen atoms.

To investigate this atypical binding motif further, we titrated an unstoppered analogue of the thread, **3b**, with the free macrocycle, H_2**3a**, and monitored the titration by ^{1}H NMR spectroscopy ($CDCl_3$) to determine the energetics of the interaction in the absence of the kinetic barrier to dissociation provided by the mechanical bond. However, there was virtually no shift in the amide protons of H_2**3a** in the presence of up to 20 equivalents of **3b** (4–80 mM) which indicates that the bimolecular association constant must be less than $5\,M^{-1}$—the approximate limit of this detection method with the large shifts typically observed through hydrogen-bonding amide groups. Interestingly, the ^{1}H NMR spectrum of the wholly covalently linked analogue H_2**4** in $CDCl_3$ also gave no indication of hydrogen-bonding interactions between the pyridine-2,6-carboxamide protons and the second pyridine residue, even though this very large macrocycle is certainly flexible enough to adopt such a geometry without steric hindrance.

Rare hydrogen-bond motifs have previously been observed within rotaxane architectures (e.g. amide NH to ester acyl oxygen atoms,[8,9] and amide NH to ester alkyl oxygen atoms[9]). The propensity for such unusual interactions in mechanically bonded structures presumably arises for a number of reasons: 1) the enforced high local concentration of functional groups for which there is a low steric cost to relative movement within the vector of the thread; 2) the limited number of conformations and co-conformations that each component can adopt that do not put functional groups into convergent orientations; 3) the imposed orthogonalization of components which can preclude normally preferred noncovalent bonding geometries; 4) freezing out of a single co-conformation for an intercomponent binding event only costs a reduction of two degrees of freedom (translation and rotation of the macrocycle about the thread) in contrast to the multiple degrees of rotational freedom of the alkyl chains that would be lost by internal hydrogen bonding in H_2**4**; 5) the inefficient solvation of internal or congested surfaces of an interpenetrated architecture means that desolvation of binding sites is likely to occur at a lower energetic cost than for conventional structures. All of these factors effectively do the same thing, that is, raise the energy of the rotaxane with respect to the free components. However, the kinetic stabilization of the architecture provided by the stoppers prevents dethreading (the rotaxane is not in equilibrium with the free components). This increase in free energy is actually a form of host preorganization, which serves to enhance binding properties as outlined by Cram over 30 years ago.[10] The result is that interactions which are not strong enough to stabilize a host–guest complex can become thermodynamically favorable if the components are held together by a mechanical bond (Figure 1).

We reasoned that it should be possible to disrupt the intercomponent hydrogen-bonding interaction in H_2**1** by protonation of the more basic 2,6-dioxymethylenepyridine nitrogen atom (Scheme 1). Although treatment of H_2**1** with one equivalent of trifluoromethanesulfonic acid (TfOH) resulted in protonation of the desired site (Figure 4d), the downfield shift of the H_C amide protons indicated that strong hydrogen bonding was still present. The shielding and broadening of particular thread signals at 298 K (Figure 4d) suggests that instead of residing over the pyridine residue as in H_2**1**, the macrocycle is displaced to the side and shuttles between the two halves of the thread relatively slowly on the

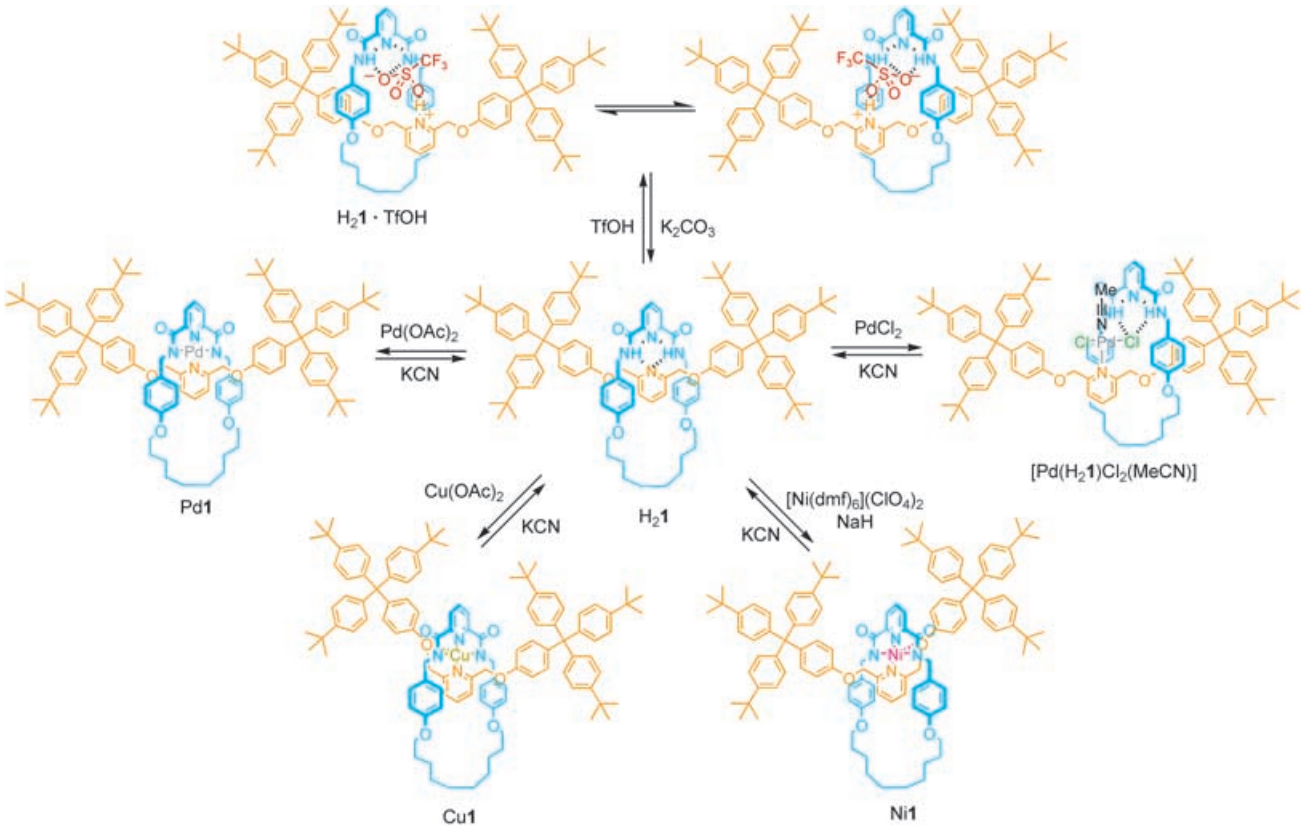

Scheme 1. Binding modes observed for [2]rotaxane H_2**1**. All of the complexation reactions are fully reversible. A similar range of complexes are exhibited by [2]catenane H_2**2** (for an X-ray crystal structure of Pd**2**, see ref. [12]). The hydrogen bonding in [Pd(H_2**1**)Cl_2(MeCN)] is observed only in the solid state. Tf = trifluoromethanesulfonyl, DMF = *N*,*N*-dimethylformamide.

NMR timescale. This was confirmed by the ^{1}H NMR spectrum recorded at 238 K (Figure 4e) in which many of the thread resonances were split into two inequivalent sets (H_b/$H_{b'}$, H_c/$H_{c'}$, H_d/$H_{d'}$, H_e/$H_{e'}$) that correspond to solvent-exposed and encapsulated (and thus magnetically shielded by the macrocycle) protons, respectively. The rationale for this behavior was provided by the crystal structure of single crystals grown from acetonitrile (Figure 5a). The [2]rotaxane acts as a host for an entire molecule of TfOH; one component (the thread) deprotonates the acid, and both components hydrogen bond to the resulting anion to generate a neutral complex, H_2**1**·HOTf. The X-ray crystal structure is consistent with the specific shielding effects seen in the ^{1}H NMR spectra, including the upfield shift of the signal for the pyridinium proton (see Figure 4c) as a consequence of other hydrogen-bond donors binding to the triflate anion, and with the noncovalent binding of the sulfonic acid acting as a transient steric barrier to shuttling of the macrocycle between the two halves of the thread.[12] In contrast (Scheme 2), a 1:1 mixture of H_2**3a** and **3b**H^+TfO^- in $CDCl_3$ shows neither upfield shift of resonances H_c, H_d, and H_e (compare Figure 4b with the spectrum of the protonated thread in Figure 4c) nor downfield shifts of the protons from the amide groups in H_2**3a**. Similarly, the absence of shifts in the amide resonances of the protonated covalently linked structure H_2**4**·H^+TfO^- suggests that it does not internally associate through hydrogen bonding.

The mechanically interlocked assemblies also differ from their noninterlocked counterparts in their ability to adopt a range of overall neutral binding modes with metals. Treatment of H_2**1** or H_2**2** with $Cu(OAc)_2$ in MeOH/CH_2Cl_2 with heating at reflux resulted in double deprotonation of the ligand and the generation of the corresponding 1:1 neutral metal-interlocked ligand complex. Recrystallization of the copper [2]rotaxane complex, Cu**1**, from acetonitrile gave single crystals that were suitable for X-ray crystallographic studies (Figure 5b). The solid-state structure shows a square-based pyramidal coordination motif that involves one of the thread oxygen atoms as well as the four nitrogen atoms of the rotaxane which form the near-planar base of the pyramid (N47 lies approximately 10° above the plane defined by N2-N11-N5-Cu). Treatment of H_2**3a**/**3b** or H_2**4** with $Cu(OAc)_2$ under the same conditions gave no indication of formation of a complex nor deprotonation of the amide groups of the macrocycle.

The synthesis of complexes of the mechanically interlocked ligands with nickel required more vigorous conditions ($[Ni(dmf)_6](ClO_4)_2$, NaH, DMF, 60 °C, 1 h) but nonetheless resulted in Ni**1** and Ni**2**, both isolated as orange crystalline compounds. In this case, a similarly colored complex could also be generated with H_2**3a**/**3b**, but unlike Ni**1** or Ni**2** the isolated compound rapidly decomposed and we were unable to isolate or characterize it. The X-ray crystal structure of single crystals of Ni**1** grown from slow cooling of a saturated

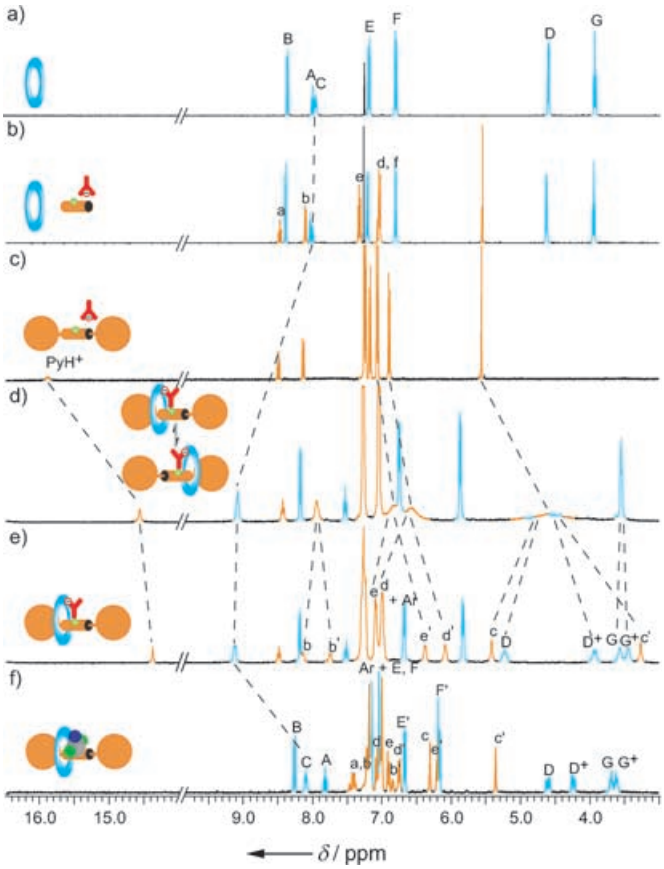

Figure 4. ^{1}H NMR spectra ($CDCl_3$, 400 MHz, 298 K unless otherwise stated): a) macrocycle H_2**3a**; b) H_2**3a** and unstoppered thread **3b** and HOTf; c) thread and HOTf (Py = pyridine); d) [2]rotaxane complex H_2**1**·HOTf showing fast exchange (shuttling) of the macrocycle between equivalent sites on both halves of the thread; e) [2]rotaxane complex H_2**1**·HOTf at 238 K showing slow exchange (reversible noncovalent bonding of the triflate anion provides a transient steric barrier to shuttling); f) [Pd(H_2**1**)Cl_2(MeCN)] showing slow exchange (coordination of [$PdCl_2$(MeCN)] provides a fixed steric barrier to shuttling up to at least 325 K). See Figure 2 for atom labeling scheme.

solution in acetonitrile is shown in Figure 5c and is closely related to the structure obtained for Cu**1**. Treatment of any of the rotaxane or catenane metal complexes with KCN in CH_2Cl_2/MeOH regenerated the original interlocked molecule, H_2**1** or H_2**2**. The differences in both the ease of formation and the stability of the metal complexes with the catenane and rotaxane relative to the noninterlocked ligands is, again,

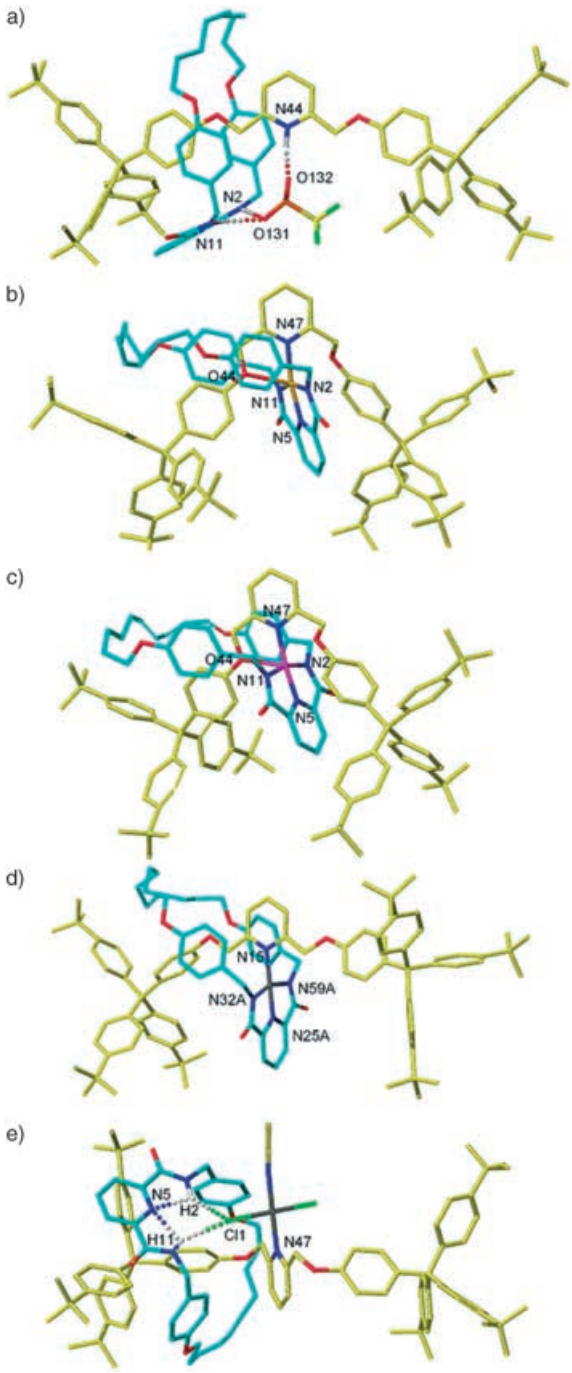

Figure 5. X-ray crystal structures[7] of various complexes of **1**: a) neutral [2]rotaxane–triflic acid complex, H_2**1**·HOTf. Note the macrocycle is displaced to one side of the central region of the thread relative to free H_2**1** (Figure 3b); b) square-pyramidal coordination complex Cu**1**; c) square-pyramidal coordination complex Ni**1**; d) square-planar coordination complex Pd**1**; e) square-planar coordination complex [Pd(H_2**1**)Cl_2(MeCN)]. C (macrocycle) turquoise; C (thread) yellow; O red; N dark blue; H white; S orange; F light green; Cl dark green; Cu tan; Ni pink; Pd dark gray. For clarity only amide hydrogen atoms are shown. Selected hydrogen-bond lengths [Å] for H_2**1**·HOTf: N2H–O131 2.14; N11H–O131 2.17; N44H–O132 1.72. Selected bond angles [°] for H_2**1**·HOTf:N2H-O131 159.0; N11H-O131 148.1; N44H-O132 159.7. Selected bond lengths [Å] for Cu**1**: N2–Cu 2.00; N11–Cu 1.98; N5–Cu 1.92; N47–Cu 2.02; O44–Cu 2.41. Selected bond angles [°] for Cu**1**: N2-Cu-N5 80.3; N5-Cu-N11 80.7; N11-Cu-N47 101.3; N5-Cu-O44 116.6; N5-Cu-N47 169.7. Selected bond lengths [Å] for Ni**1**: N2–Ni 1.94; N11–Ni 1.93; N5–Ni 1.81; N47–Ni 1.93; O44-Cu 2.52. Selected bond angles [°] for Ni**1**: N2-Ni-N5 82.6; N5-Ni-N11 82.4; N11-Ni-N47 98.5; N5-Ni-O44 113.8; N5-Ni-N47 172.1. Selected bond lengths [Å] for Pd**1**: Pd–N15 1.95, Pd–N25 1.86, Pd–N32 2.04, Pd–N59 2.02, N15–N25 3.81. Selected bond angles [°] for Pd**1** N59-Pd-N32 160.0. Selected bond lengths [Å] for [Pd(H_2**1**)Cl_2(MeCN)]: Pd–N47 1.98, Pd–Cl1 2.27, Cl1–H2 2.67, Cl1–H11 2.64, N5–H2 2.36, N5–H11 2.15. Selected bond angles [°] for [Pd(H_2**1**)Cl_2(MeCN)]: N2-H2-Cl1 139.8, N11-H11-N5 114.1, N11-H11-Cl1 125.0.

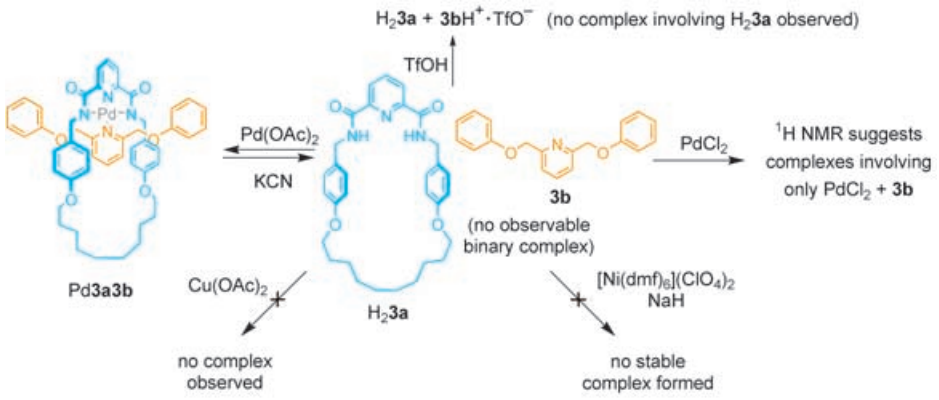

Scheme 2. Attempted complexation experiments involving H_2**3a**/**3b**. Similar results were obtained with macrocycle H_2**4** (for an X-ray crystal structure of Pd**4**, see ref. [12]).

consistent with the intrinsic effect of kinetic stabilization of a mechanically interlocked architecture (Figure 1c).

Each of the four ligand sets reacts with $Pd(OAc)_2$ (H_2**1**, H_2**2**, and H_2**4** directly in $MeCN/CH_2Cl_2$; H_2**3a**/**3b** requires preliminary reaction of $Pd(OAc)_2$ with H_2**3a** in MeCN followed by treatment of the resulting complex with **3b** in CH_2Cl_2) to give the corresponding square-planar coordination complexes (Schemes 1 and 2 and Figure 5d). However, the rotaxane and catenane also formed a different type of neutral square-planar coordination complex when treated with $PdCl_2$, an initial palladium salt that features significantly stronger coordinating ligands (chloride is also less basic than acetate). Slow cooling of saturated solutions of either complex in acetonitrile afforded crystals that were suitable for X-ray crystallography, and the structure of the rotaxane complex, $[Pd(H_2\mathbf{1})Cl_2(MeCN)]$, is shown in Figure 5e (the solid-state structure of the [2]catenane complex is similar but features intermolecular rather than intramolecular NH···Cl–Pd hydrogen bonding). From the crystal structures it can be seen that although Pd coordinates to the thread as in Pd**1**, the original metal chloride ligands remain intact and the macrocycle amides are not deprotonated. In solution the coordination of the $[PdCl_2(MeCN)]$ unit to the pyridine ring of the thread acts as a steric barrier to shuttling (Figure 4f). This is similar to the effect seen with H_2**1**·TfOH, but unlike the complex held together by hydrogen bonds the coordination to the metal is not kinetically labile and persists as a barrier to shuttling up to at least 325 K (close to the boiling point of the solvent $CDCl_3$).[11]

The solid-state structure of $[Pd(H_2\mathbf{1})Cl_2(MeCN)]$ features hydrogen bonding between the amide groups of the macrocycle and the chloride ligands of the metal (Figure 5e). However, the ^{1}H NMR spectrum shows that this interaction is not present to any significant extent in $CDCl_3$ (the chemical shift of H_C is virtually unchanged compared to H_2**3a**; Figure 4f). Wisner and co-workers recently used a similar interaction to direct an elegant synthesis of a pseudorotaxane.[13] During the course of that work, a macrocycle binding constant that largely results from two sets of isophthalamide groups hydrogen bonding to the chloride ligands of a Pd^{II} complex was determined to be $5\times10^3\,M^{-1}$ in $CDCl_3$.[13] In contrast, Crabtree and co-workers determined the association constant for a single isophthalamide group with Cl^- to be $6\times10^4\,M^{-1}$ in CD_2Cl_2.[14] Accordingly, a C(O)NH···Cl–Pd interaction must be somewhat less than half the strength of a C(O)NH···Cl^- hydrogen bond. This is consistent with the observation that the interaction is too weak to significantly bind the macrocycle in $[Pd(H_2\mathbf{1})Cl_2(MeCN)]$ in $CDCl_3$, despite the high effective molarity introduced by the mechanical bond, and is in marked contrast to the effective bifurcated pyridine–pyridine hydrogen bonding in H_2**1**. This suggests that the intercomponent binding mode in H_2**1** is not particularly weak and its scarcity as an observed interaction may arise because the geometry of the interlocked architecture precludes otherwise preferred noncovalent bonding geometries.

In conclusion, the kinetically enforced association of molecular fragments within an interlocked architecture facilitates the formation of diverse, and sometimes rare and unusual, binding motifs both in solution and the solid state. These interactions can produce interesting effects in their own right; the cooperative hydrogen bonding of an organic guest by both components of a [2]rotaxane can present an effective barrier to shuttling at low temperatures, whereas a stronger metal–ligand coordination mode can be used to restrict the same motion even at higher temperatures. The fact that many of the observed modes of binding are weaker or not seen at all when the components are not mechanically interlocked makes this consequence of the mechanical bond particularly noteworthy.[15]

Received: January 1, 2005
Revised: February 18, 2005
Published online: June 23, 2005

Keywords: catenanes · coordination modes · hydrogen bonds · noncovalent interactions · rotaxanes

[1] For reviews, see: a) *Molecular Catenanes, Rotaxanes, and Knots: A Journey Through the World of Molecular Topology* (Eds.: J.-P. Sauvage, C. Dietrich-Buchecker), Wiley-VCH, Weinheim, **1999**; b) V. Balzani, A Credi, F. M. Raymo, J. F. Stoddart, *Angew. Chem.* **2000**, *112*, 3484–3530; *Angew. Chem. Int. Ed.* **2000**, *39*, 3348–3391; c) V. Balzani, M. Venturi, A. Credi, *Molecular Devices and Machines—A Journey into the Nanoworld*, Wiley-VCH, Weinheim, **2003**; d) A. H. Flood, R. J. A. Ramirez, W.-Q. Deng, R. P. Muller, W. A. Goddard, J. F. Stoddart, *Aust. J. Chem.* **2004**, *57*, 301–322; e) "Synthetic Molecular Machines": E. R. Kay, D. A. Leigh in *Functional Artificial Receptors* (Eds.: T. Schrader, A. D. Hamilton), Wiley-VCH, Weinheim, **2005**, 333–406.

[2] For examples in which encapsulation and/or preorganization of the coordinating ligand geometry in a mechanically interlocked architecture can bring about significant property effects, see: (stabilization of oxidation state/complex geometry) a) C. O. Dietrich-Buchecker, J.-P. Sauvage, *J. Am. Chem. Soc.* **1984**, *106*, 3043–3045; b) N. Armaroli, L. De Cola, V. Balzani, J.-P. Sauvage, C. O. Dietrich-Buchecker, J.-M. Kern, A. Bailal, *J. Chem. Soc. Dalton Trans.* **1993**, 3241–3247; (protection of functional groups) c) D. Leigh, A. Murphy, J. P. Smart, A. M. Z. Slawin, *Angew. Chem.* **1997**, *109*, 752–756; *Angew. Chem. Int. Ed. Engl.* **1997**, *36*, 728–731; d) M. R. Craig, M. G. Hutchings, T. D. W. Claridge, H. L. Anderson, *Angew. Chem.* **2001**, *113*, 1105–1108; *Angew. Chem. Int. Ed.* **2001**, *40*, 1071–1074; e) J. E. H. Buston, F. Marken, H. L. Anderson, *Chem. Commun.* **2001**, 1046–1047; f) T. Oku, Y. Furusho, T. Takata, *Org. Lett.* **2003**, *5*, 4923–4925; g) D. A. Leigh, E. M. Pérez, *Chem. Commun.* **2004**, 2262–2263; (solubility) h) H. W. Gibson, S Liu, P. Lecavalier, C. Wu, Y. X. Shen, *J. Am. Chem. Soc.* **1995**, *117*, 852–874; i) A. G. Johnston, D. A. Leigh, A. Murphy, J. P. Smart, M. D. Deegan, *J. Am. Chem. Soc.* **1996**, *118*, 10662–10663; j) S. Anderson, H. L. Anderson, *Angew. Chem.* **1996**, *108*, 2075–2078; *Angew. Chem. Int. Ed. Engl.* **1996**, *35*, 1956–1959; (conformation of a component) k) W. Clegg, C. Gimenez-Saiz, D. A. Leigh, A. Murphy, A. M. Z. Slawin, S. J. Teat, *J. Am. Chem. Soc.* **1999**, *121*, 4124–4129; (electroluminescence) l) F. Cacialli, J. S. Wilson, J. J. Michels, C. Daniel, C. Silva, R. H. Friend, N. Severin, P. Samori, J. P. Rabe, M. J. O'Connell, P. N. Taylor, H. L. Anderson, *Nat. Mater.* **2002**, *1*, 160–164; (membrane transport) m) V. Dvornikovs, B. E. House, M. Kaetzel, J. R. Dedman, D. B. Smithrud, *J. Am. Chem. Soc.* **2003**, *125*, 8290–8301.

[3] A.-M. Fuller, D. A. Leigh, P. J. Lusby, I. D. H. Oswald, S. Parsons, D. B. Walker, *Angew. Chem.* **2004**, *116*, 4004–4008; *Angew. Chem. Int. Ed.* **2004**, *43*, 3914–3918.

[4] For a recent example of a [2]rotaxane that utilizes square-planar Pd^{II} coordination, see: I. Yoon, M. Narita, T. Shimizu, M. Asakawa, *J. Am. Chem. Soc.* **2004**, *126*, 16740–16741.

[5] S. L. Jain, P. Bhattacharyya, H. L. Milton, A. M. Z. Slawin, J. A. Crayston, J. D. Woollins, *Dalton Trans.* **2004**, 862–871.

[6] F. Biscarini, M. Cavallini, D. A. Leigh, S. León, S. J. Teat, J. K. Y. Wong, F. Zerbetto, *J. Am. Chem. Soc.* **2002**, *124*, 225–233.

[7] Structural data for H_2**1**, Cu**1**, and Ni**1** were collected at 93 K using a Rigaku Saturn diffractometer (MM007 high-flux RA/$Mo_{K\alpha}$ radiation, confocal optic); for H_2**2** and $[Pd(H_2\mathbf{1})Cl_2$-(MeCN)] at 93 K using a Rigaku Mercury diffractometer (MM007 high-flux RA/$Mo_{K\alpha}$ radiation, confocal optic); and for H_2**1**·TfOH at 125 K using a Bruker SMART diffractometer (sealed tube $Mo_{K\alpha}$ radiation, graphite monochromator, $\lambda = 0.71073$ Å). All data collections employed narrow frames (0.3–1.0°) to obtain at least a full hemisphere of data. Intensities were corrected for Lorentz polarization and absorption effects (multiple equivalent reflections). Structures were solved by direct methods, non-hydrogen atoms were refined anisotropically with CH protons being refined in riding geometries (SHELXTL) against F^2. In most cases, amide protons were refined isotropically subject to a distant constraint. Any other restraints or additional features of the refinement are detailed for each structure below. The structure determination for H_2**1** proved particularly problematic; we collected full datasets using a variety of collection routines on more than 15 different crystals from several different crystallization experiments. The data were always poor, principally because of disorder arising from the alkyl chain and solvated molecules. The structure was refined isotropically with no protons included in the refinement. H_2**1**: $C_{112}H_{130}N_4O_6$, $M_r = 1628$, crystal size $= 0.2 \times 0.1 \times 0.03$ mm^3, orthorhombic, *Pbca*, $a = 18.338(4)$, $b = 23.545(5)$, $c = 44.922(9)$ Å, $V = 19396(7)$ Å^3, $Z = 8$, $\rho_{calcd} = 1.115$ Mg m^{-3}; $\mu = 0.068$ mm^{-1}, 18573 data (17303 unique), $R = 0.3339$ for F values of reflections with $F_o > 4\sigma F_o$), $S = 4.90$ for 463 parameters. Residual electron density extremes were 1.665 and −4.557 eÅ^{-3}. H_2**2**: $C_{62}H_{76}N_4O_8$, $M_r = 1005.27$, colorless prism, crystal size $= 0.2 \times 0.2 \times 0.2$ mm^3, triclinic, *P*-1, $a = 11.3539(11)$, $b = 12.0635(11)$, $c = 20.445(2)$ Å, $\alpha = 82.323(6)$, $\beta = 88.351(7)$, $\gamma = 80.397(7)$°, $V = 2736.2(5)$ Å^3, $Z = 2$, $\rho_{calcd} = 1.220$ Mg m^{-3}; $\mu = 0.080$ mm^{-1}, 15494 data (8824 unique, $R_{int} = 0.0176$), $R = 0.0499$, $S = 0.987$ for 677 parameters. Residual electron density extremes were 0.759 and −0.336 eÅ^{-3}. H_2**1**·TfOH: $C_{113}H_{131}F_3N_4O_9S$, $M_r = 1778.28$, colorless prism, crystal size $= 0.15 \times 0.1 \times 0.1$ mm^3, monoclinic, $P2_1/c$, $a = 20.555(2)$, $b = 18.7503(19)$, $c = 27.853(3)$ Å, $\beta = 109.574(2)$°, $V = 10114.6(17)$ Å^3, $Z = 4$, $\rho_{calcd} = 1.168$ Mg m^{-3}; $\mu = 0.096$ mm^{-1}, 59606 data (18472 unique, $R_{int} = 0.0449$), $R = 0.1058$, $S = 1.028$ for 1149 parameters. Residual electron density extremes were 1.366 and −0.649 eÅ^{-3}. Cu**1**: $C_{117}H_{135.5}CuN_{6.5}O_6$, $M_r = 1792.36$, violet platelet, crystal size $= 0.2 \times 0.1 \times 0.01$ mm^3, triclinic, *P*-1, $a = 16.404(3)$, $b = 17.516(3)$, $c = 20.046(4)$ Å, $\alpha = 100.573(3)$, $\beta = 106.016(3)$, $\gamma = 96.178(3)$°, $V = 5365.3(17)$ Å^3, $Z = 2$, $\rho_{calcd} = 1.109$ Mg m^{-3}; $\mu = 0.258$ mm^{-1}, 41166 data (17787 unique, $R_{int} = 0.0318$), $R = 0.1507$, $S = 1.812$ for 1163 parameters. Residual electron density extremes were 2.325 and −1.107 eÅ^{-3}. The half-weight acetonitrile solvent molecules were refined isotropically. Ni**1**: $C_{117}H_{137.5}N_{6.5}NiO_7$, $M_r = 1805.54$, orange needle, crystal size $= 0.15 \times 0.015 \times 0.015$ mm^3, triclinic, *P*-1 $a = 16.423(3)$, $b = 17.582(3)$, $c = 20.056(3)$ Å, $\alpha = 100.0161(19)$, $\beta = 106.234(3)$, $\gamma = 96.2695(18)$°, $V = 5398.6(15)$ Å^3, $Z = 2$, $\rho_{calcd} = 1.111$ Mg m^{-3}; $\mu = 0.235$ mm^{-1}, 40853 data (17841 unique, $R_{int} = 0.0506$), $R = 0.1302$, $S = 1.465$ for 1184 parameters. Residual electron density extremes were 1.874 and −0.891. The half-weight acetonitrile and quarter-weight water solvent molecules were refined isotropically. The protons on all solvated molecules were discounted in the refinement. $[Pd(H_2\mathbf{1})Cl_2(MeCN)]$: $C_{122}H_{145}N_9O_6Cl_2Pd$, $M_r = 2010.77$, yellow platelet, crystal size $= 0.2 \times 0.1 \times 0.01$ mm^3, monoclinic, *C*2/*c*, $a = 29.6525(12)$, $b = 23.2314(10)$, $c = 32.6559(14)$ Å, $\beta = 99.071(3)$°, $V = 22214.3(16)$ Å^3, $Z = 8$, $\rho_{calcd} = 1.202$ Mg m^{-3}; $\mu = 0.273$ mm^{-1}, 58779 data (19158 unique, $R_{int} = 0.1733$), $R = 0.1416$, $S = 1.090$ for 1253 parameters. Residual electron density extremes were 0.946 and −0.925 eÅ^{-3}. The half-weight acetonitrile solvent molecules were refined isotropically. The protons on solvated molecules were discounted in the refinement. CCDC 259162–259166 contain the supplementary crystallographic data for this paper. These data can be obtained free of charge from the Cambridge Crystallographic Data Centre via www.ccdc.cam.ac.uk/data_request/cif.

[8] F. G. Gatti, D. A. Leigh, S. A. Nepogodiev, A. M. Z. Slawin, S. J. Teat, J. K. Y. Wong, *J. Am. Chem. Soc.* **2001**, *123*, 5983–5989.

[9] J. S. Hannam, S. M. Lacy, D. A. Leigh, C. G. Saiz, A. M. Z. Slawin, S. G. Stitchell, *Angew. Chem.* **2004**, *116*, 3322–3326; *Angew. Chem. Int. Ed.* **2004**, *43*, 3260–3264.

[10] D. J. Cram, *Angew. Chem.* **1988**, *100*, 1041 – 1052; *Angew. Chem. Int. Ed. Engl.* **1988**, *27*, 1009 – 1020.
[11] For temporary steric barriers to shuttling, see: a) A. S. Lane, D. A. Leigh, A. Murphy, *J. Am. Chem. Soc.* **1997**, *119*, 11092 – 11093; b) L. Jiang, J. Okano, A. Orita, J. Otera, *Angew. Chem.* **2004**, *116*, 2173 – 2176; *Angew. Chem. Int. Ed.* **2004**, *43*, 2121 – 2124.
[12] A.-M. L. Fuller, D. A. Leigh, P. J. Lusby, A. M. Z. Slawin, D. B. Walker, unpublished results.
[13] B. A. Blight, K. A. Van Noortwyck, J. A. Wisner, M. C. Jennings, *Angew. Chem.* **2005**, *117*, 1523 – 1528; *Angew. Chem. Int. Ed.* **2005**, *44*, 1499 – 1504.
[14] K. Kavallieratos, S. R. de Gala, D. J. Austin, R. H. Crabtree, *J. Am. Chem. Soc.* **1997**, *119*, 2325 – 2326.
[15] *Note added in proof*: A paper recently appeared (Y. Furusho, T. Matsuyama, T. Takata, T. Moriuchi, T. Hirao, *Tetrahedron Lett.* **2004**, *45*, 9593 – 9597) that reproduces some of the previous work[3] on the square-planar template rotaxane system. Although the authors do not comment on it, the ^{1}H NMR chemical shifts show that the bifurcated pyridine–pyridine hydrogen-bonding motif also exists in their demetalated rotaxane.

